N-, O-, and S-Tridoped Nanoporous Carbons as Selective Catalysts for Oxygen Reduction and Alcohol Oxidation Reactions

Yuying Meng,[†,‡] Damien Voiry,[∥] Anandarup Goswami,[†,⊥] Xiaoxin Zou,[§] Xiaoxi Huang,[⊥] Manish Chhowalla,[∥] Zhongwu Liu,*[,‡] and Tewodros Asefa*[,†,⊥]

[†]Department of Chemical and Biochemical Engineering, [⊥]Department of Chemistry and Chemical Biology, [∥]Department of Materials Science and Engineering, Rutgers, The State University of New Jersey, Piscataway, New Jersey 08854, United States

[‡]School of Materials Science and Engineering, South China University of Technology, 381 Wushan Road, Tianhe District, Guangzhou 510640, China

[§]State Key Laboratory of Inorganic Synthesis & Preparative Chemistry, College of Chemistry, Jilin University, 2699 Qianjin Street, Changchun 130012, China

S *Supporting Information*

ABSTRACT: Replacing rare and expensive metal catalysts with inexpensive and earth-abundant ones is currently among the major goals of sustainable chemistry. Herein we report the synthesis of N-, O-, and S-tridoped, polypyrrole-derived nanoporous carbons (NOSCs) that can serve as metal-free, selective electrocatalysts and catalysts for oxygen reduction reaction (ORR) and alcohol oxidation reaction (AOR), respectively. The NOSCs are synthesized via polymerization of pyrrole using $(NH_4)_2S_2O_8$ as oxidant and colloidal silica nanoparticles as templates, followed by carbonization of the resulting S-containing polypyrrole/silica composite materials and then removal of the silica templates. The NOSCs exhibit good catalytic activity toward ORR with low onset potential and low Tafel slope, along with different electron-transfer numbers, or in other words, different ratios H_2O/H_2O_2 as products, depending on the relative amount of colloidal silica used as templates. The NOSCs also effectively catalyze AOR at relatively low temperature, giving good conversions and high selectivity.

The practical large-scale applications of many useful catalytic and electrocatalytic systems are currently constrained by the lack of sustainable/inexpensive (electro)catalysts composed of earth-abundant elements. Notable examples of such systems include fuel cells, where the most effective catalysts for these important energy conversion systems still remain noble metal-based materials, e.g., Pt/C.[1] Hence inexpensive and sustainable catalytic materials are critically needed to make fuel cells widely applicable.[2] Recently, efforts to tackle these issues have been gaining more traction, with reports of various nonprecious metal or metal-free materials, such as N-doped nanocarbons, that can catalyze reactions that were previously known to be catalyzed only by noble metals. In particular, the revelations that heteroatom-doped carbon materials show catalytic activity toward the oxygen reduction reaction (ORR), the hydrogen evolution reaction (HER), and the oxygen evolution reaction (OER) with comparable efficiency as noble metal-based catalysts have triggered a race among researchers to find other "unconventional" or sustainable materials with similar, or not

better, catalytic activity.[3] Moreover, the very fact that a simple doping of carbon materials by heteroatoms (e.g. N, S, B, and P) can make these materials highly effective catalysts[4] currently calls for more research in this area.

At this juncture, finding new synthetic methods that can lead to carbon-based materials with better structures, and thereby more favorable catalytic properties, is of utmost interest. As high surface area often makes catalysts more effective,[5] not surprisingly many of the heteroatom-doped carbons reported before are made with high surface area, typically via nanocasting using porous materials such as mesoporous silica as templates. However, other templating synthetic strategies, which could lead to carbon materials with high porosity, good electrochemical contact area, and better diffusion pathways, for substrates/products should be explored as well. Moreover, methods that can co-introduce different types of heteroatom dopants within carbon nanomaterials and the properties of the resulting materials for electrocatalysis are also worth investigating. Following the same thoughts, herein we report the synthesis of metal-free, N-, O- and S-tridoped polypyrrole-derived nanoporous carbons (NOSCs) that show efficient and selective (electro)catalytic activity in ORR and AOR (Scheme 1).

Scheme 1. Synthetic Procedures Used to Make NOSCs

Colloidal Silica   S-PPY-silica   NOSCs
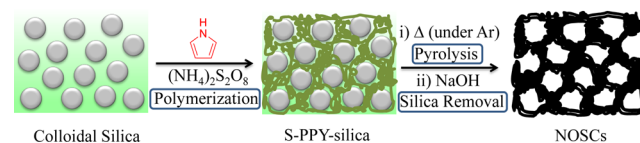
The synthesis involves three steps: (1) polymerization of pyrrole in the presence of colloidal silica templates using $(NH_4)_2S_2O_8$ as oxidant, as reported by Maeda and Armes,[6] (2) pyrolysis of the resulting S-containing polypyrrole-silica (S-PPY-silica) composite material, and (3) removal of the silica templates from the carbonized material using aqueous NaOH solution (see Supporting Information, SI, for more details). By varying the synthetic conditions and the relative amount of silica nano-

particles and PPY, NOSCs with different densities of N, O, and S dopants are finally obtained. The ratios of PPY to silica in the S-PPY-silica precursors, in which the two are presumably bound via hydrogen bonding, are confirmed by TGA (Figure S1 and Table S1).

The resulting nanoporous carbon materials are labeled as NOSC$_x$-T, where x represents the amount of colloidal silica in g (0.5, 2, 4, or 8) for 9.2 mmol pyrrole and T represents the final pyrolysis temperature (600, 700, 800, 900, or 1000 °C) used for the synthesis of the materials. While the PPY is used as a carbon precursor and a source of N dopant atoms, the persulfate is used as a source of S and O dopants in the NOSC materials (besides serving as oxidant for polymerization of pyrrole into PPY). For comparison, control materials, namely N-, O-, and S-tridoped PPY-derived *carbon black* with different densities of N, S, and O dopants (NOSCB-900(A) and NOSPCB-900(B)) are prepared without using colloidal silica templates (see SI).

Representative results of N$_2$ adsorption/desorption isotherms and TEM images of the carbon materials synthesized above are shown in Figures S2 and S3 and also discussed in detail in SI and Table S2. Their Raman spectra (Figure S4) show peaks at 1360 and 1586 cm^{-1}, corresponding to the characteristic D and G bands, respectively, of graphitic carbons.[4] As the G band is related to tangential vibrations of sp^2 carbon atoms,[7] its presence on the spectra is suggestive of the existence of graphitic structure in NOSCs. On the other hand, the D band, which corresponds to the defect band, must be due to the presence of N, O, and/or S dopant atoms and the concomitant absence of some graphitic carbons in the NOSC materials. By obtaining the ratio of intensities of the two bands (i.e., I_D/I_G),[8] the relative degree of order/disorder in the NOSC materials is then determined. In the case of NOSC$_8$-T (materials synthesized using different pyrolysis temperatures but the same amount of colloidal silica), the I_D/I_G ratio decreases from 1.12 to 0.94 when the pyrolysis temperature is raised from 600 °C to 1000 °C (Figure S4a,b); this indicates the increase in the degree of ordered graphitic structure in materials prepared at higher pyrolysis temperatures.[9] However, the I_D/I_G ratio of the NOSC$_x$-900 (materials synthesized at the same temperature but with different amounts of silica) remains almost the same, suggesting their similar content of graphitic (or defect) structures irrespective of the amount of colloidal silica used for their synthesis (Figure S4c,d).

The XPS survey spectra of NOSC$_8$-T materials (Figure S5) show three prominent peaks associated with C 1s, N 1s, and O 1s electrons as well as a minor peak associated with S 2p electrons, indicating the presence of N, O, and S dopants in the materials. The elemental compositions of the materials determined by XPS (Table S2) are used for the discussions below on structure−property correlations of the materials, as the surface atoms matter most for the catalytic reactions we studied here. In addition, our elemental analyses data (Table S3) also seem to correlate well with the XPS results. The N:C atomic ratio is found to significantly decrease (from 0.27 to 0.04) when the pyrolysis temperature is increased from 600 °C to 1000 °C (Figure 1a). Similarly, the O:C and S:C atomic ratios are found to decrease (from 0.09 to 0.04 and from 0.02 to 0.01, respectively) when the pyrolysis temperature is increased from 600 to 1000 °C.

Figure S6 shows high-resolution N 1s XPS peaks of NOSC$_8$-T materials, which are further deconvoluted into four peaks corresponding to pyridinic-N (397.9 eV), pyrrolic-N (399.1 eV), quaternary-N (400.0 eV), and pyridinic-N$^+$-O$^-$ (403.0 eV) species.[2] As the pyrolysis temperature to make the materials is raised from 600 to 1000 °C, the percentage of quaternary-N
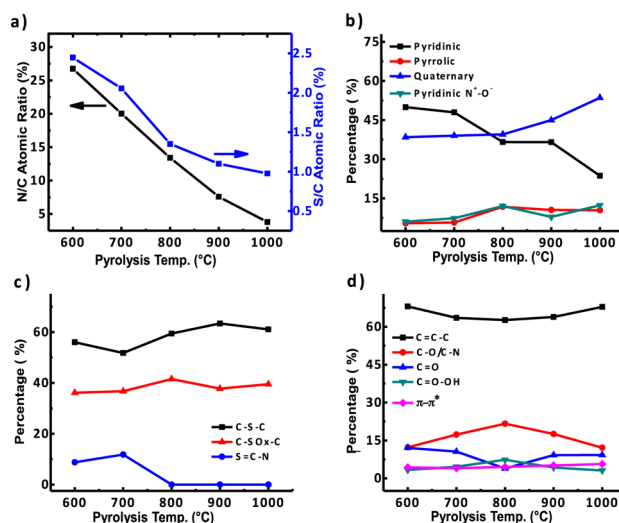

Figure 1. Composition of NOSC$_8$-T materials as a function of their pyrolysis temperatures: (a) N/C, O/C and S/C atomic ratios and percentages of the different (b) N, (c) S, and (d) C species present in NOSC$_8$-T materials.

increases, but that of pyridinic-N decreases, while those of pyrrolic-N and pyridinic-N$^+$-O$^-$ species remain almost the same (Figure 1b). The high resolution S 2p peaks are also deconvoluted, mainly into two peaks associated with C−S−C (163.8/165.1 eV) and C−SO$_x$−C (167.3/168.6 eV) species.[10] In the case of NOSC$_8$-600 and NOSC$_8$-700, the S 2p signals further contain a minor peak at lower binding energy possibly corresponding to S=C−N species (∼10% of total S content). On the other hand, the materials prepared at higher temperatures contain a higher amount of C−S−C groups (Figure 1c)−chem-−chemical species that are deemed more catalytically active for ORR.[4] In case of high-resolution C 1s spectra of the materials (Figure S7), peaks corresponding to C=C−C (284.6 eV), C−O/C−N (286.1 eV), C=O (287.5 eV), and C=O−OH (289.2 eV) moieties and a π−π^* satellite peak (290.6 eV) are observed.[11] Needless to say, many of these peaks indicate the presence of O and N dopants in the materials as well.

With regard to NOSC$_x$-900, the XPS spectra show a steady increase in the amount of O dopants at the expense of N and S dopants as the amount of colloidal silica used in the synthesis of the materials increases (see Table S2). This clearly indicates that the silica nanoparticles used as templates for synthesis of NOSCs may have provided some of the O dopants or catalyze O doping into the NOSCs.[2]

The electrocatalytic activities of NOSCs and the control materials (i.e., NOSCB-900(A) and NOSCB-900(B)) toward ORR were then evaluated. Since NOSC$_8$-900 is ultimately found to be the most ORR active catalyst among the NOSC materials we synthesized and studied, it is chosen for most of the discussions here. The cyclic voltammograms (CVs) at a scan rate of 100 mV/s on NOSC$_8$-900 (Figure 2a) show a strong cathodic peak at 0.75 V vs reversible hydrogen electrode (RHE) in O$_2$-saturated electrolyte, but expectedly show no response in the same potential range in N$_2$-saturated electrolyte. This indicates NOSC$_8$-900's electrocatalytic activity toward ORR. The material's high activity for ORR is gleaned from its high positive onset potential value of ∼0.96 V vs RHE and half-wave potential ($E_{1/2}$) value of ∼0.74 V vs RHE. These values are comparable with those of Fe/Ni-containing N-doped carbon nanotubes, which are recently reported as among the best ORR electro-
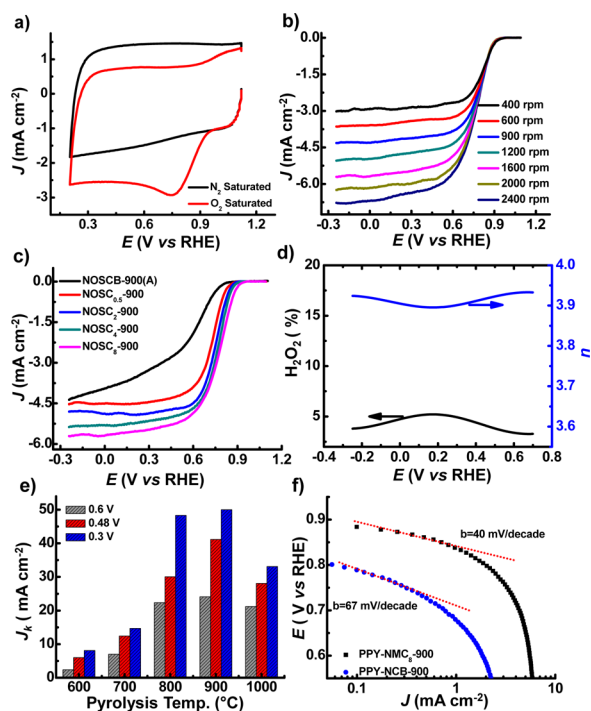
Figure 2. (a) CVs of NOSC$_8$-900 in O$_2$- and N$_2$-saturated 0.1 M KOH solutions, (b) polarization curves of ORR over NOSC$_8$-900 on RDE rotating at different speeds, (c) polarization curves of ORR over NOSC$_x$-900 materials on RDE rotating at 1600 rpm, (d) electron-transfer number and H$_2$O$_2$ yield in ORR on NOSC$_8$-900 material, (e) kinetic current density (J_k) of ORR at different potentials on NOSC$_8$-T materials, and (f) Tafel plots of NOSC$_8$-900 and NOSCB-900(A) at 1600 rpm.

catalysts.[12] Moreover, the mass activity of NOSC$_8$-900 is 7.4 A g^{-1} at 0.8 V vs RHE, which is higher than some of the most efficient ORR electrocatalysts reported recently, e.g., carbon nanotube-graphene composite material, which gives a mass activity of 4.4 A g^{-1} at 0.8 V vs RHE.[13] The control materials NOSCB-900(A) and NOSCB-900(B) also show cathodic peaks associated with ORR, but they do so at much higher overpotentials (onset potential ≈ 0.54−0.57 V) (Figure S9). Moreover, NOSCB-900(A) shows a slightly better electro-catalytic activity for ORR (with E_{peak} ≈ 0.57 V vs RHE and J ≈ 2.0 mA cm^{-2}) compared with NOSCB-900(B) (which gives E_{peak} ≈ 0.54 V and J ≈ 1.3 mA cm^{-2}) (Figure S9). Since NOSCB-900(A) has reasonably similar surface area as NOSCB-900(B) but higher amount of S and O dopants than NOSCB-900(B) (Table S2), NOSCB-900(A)'s better activity than NOSCB-900(B) suggests that having S and O codopants within N-doped carbon nanomaterials significantly improves the electrocatalytic activity of the latter toward ORR. Such heteroatom codopants are known to synergistically lead to asymmetric spins and better charged structures in carbon nanomaterials, and thereby better electro-catalytic properties.[14] On the other hand, NOSC$_8$-900's higher electrocatalytic activity compared with those of NOSCB-900 materials is most likely due to its larger surface area, more accessible structure, and higher amount of O dopants.

Linear sweep voltammetry (LSV) using a RDE at a scan rate of 10 mV/s showed that the current density or electrocatalytic response of the NOSC$_x$-900 materials (which have different porosity) increases as the potential increases (Figures 2b and S10). More importantly, as the amount of colloidal silica templates increases, the onset potential of the NOSC$_x$-900

materials gradually shifts to a more positive value, and their current density (J) significantly increases (Figure 2c). Notably, NOSC$_8$-900 gives the highest electrocatalytic activity toward ORR with the most positive onset potential (~0.96 V vs RHE) and the largest current density, even better than some of the best ORR catalysts reported previously.[15] It is worth adding that the activity of NOSC$_8$-900 in ORR is also comparable with that of Pt/C (20 wt. % Pt) (Figure S11). Since the total amount of dopants (O + N + S) is similar in all of NOSC$_x$-900 materials, NOSC$_8$-900's efficient electrocatalytic activity for ORR is also most likely due to its large surface area (Table S2).

The Koutecky−Levich (K-L) plots of NOSC$_x$-900 materials in ORR (Figure S10) exhibit good linearity, indicating a first-order reaction.[16] Using RDE current density as well as K-L plots, the electron-transfer number per oxygen molecule (n) in ORR over NOSC$_8$-900 and NOSC$_4$-900 is obtained to be ~4.0 (Figures 2d and S12), indicating a four-electron process, over a wide potential range. Interestingly though, n decreases to well below 4.0 as the amount of colloidal silica used for the synthesis of the materials decreases (Figure S12). In other words, the four-electron process becomes less favorable for NOSCs possessing lower porosity and/or O dopants.

To further investigate the catalytic pathways of ORR occuring on the NOSC materials, the values of n and amount of H$_2$O$_2$ formed in the ORR are determined with RDE (Figures 2d and S13). Notably, the ORR over NOSC$_8$-900 yields only <5% H$_2$O$_2$ over a wide potential range (−0.25 to 0.7 V vs RHE), consistent with the four-electron process (Figure 2d). On the other hand, NOSCB-900(A), whose n ranges from 3.2 to 3.4 (Figure S13), gives ~30−40% H$_2$O$_2$ under identical conditions (Figure S12). NOSCB-900(B), whose n is <3, gives even higher amount of H$_2$O$_2$ (~56−66%) in the reaction (Figure S14).

Further LSV studies were carried out to determine if the pyrolysis temperature affects the materials' electrocatalytic activity. Based on current densities obtained for NOSC$_8$-T materials, it can be concluded that NOSCs' electrocatalytic activity for ORR improves as the pyrolysis temperature is raised from 600 to 900 °C but decreases as the temperature is further increased from 900 to 1000 °C (Figures 2e and S15−S17). In other words, this result indicates once again that NOSC$_8$-900 is the best electrocatalyst for ORR, giving not only the most positive onset potential but also the highest kinetic current density. NOSC$_8$-900's excellent activity for ORR is also confirmed by its low Tafel slope (40 mV/decade) (Figure 2f). NOSC$_8$-900's highest electrocatalytic performance can be attributed to the materials' relatively highest proportions of most catalytically active groups for ORR (e.g., C−S−C type sulfur and pyrrolic and quaternary nitrogen species) and its large surface area, both of which in turn can give rise to more favorable electron-transfer processes during the electrocatalytic reactions.[2,4,17]

To corroborate some of the findings above, graphs of n as well as percentage of peroxide (mol H$_2$O$_2$/mol H$_2$O) formed at three different potentials vs amount of colloidal silica used as templates are plotted for the materials (Figure 3). The results show that the materials synthesized with higher amounts of colloidal silica, or have a larger density of O dopants and greater porosity, give a higher value of n and lower amount of H$_2$O$_2$ (or higher amount of H$_2$O) as product, as summarized in Scheme S1. This might be because ORR can go through a 2e + 2e pathway, as proposed by Atanassov group,[18] and the intermediate product of the first 2e process (i.e., H$_2$O$_2$) might not have as much chance to undergo the second 2e process in the low surface area NOSC materials, or
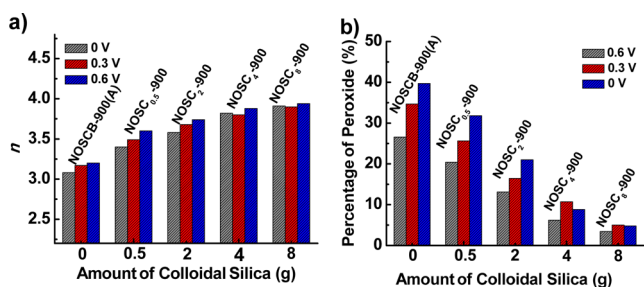
Figure 3. (a) Electron-transfer number (n) and (b) % peroxide formed at three different potentials vs amount of colloidal silica used as templates for a series of NOSC$_x$-900 materials and NOSCB-900(A).

not as much as it could in the large surface area NOSCs. Moreover, carbon materials possessing more oxygen species are known to favor the 2e process in ORR.[19] Additionally, due to the differences in their dopant content, the combined synergistic effect by N, S, and O dopants in the NOSC materials could vary, rendering them different work functions.[20] This, in turn, makes the materials to donate electrons to either the oxygen or the peroxide intermediates adsorbed on the materials' surfaces differently, resulting in different selectivity in ORR.

The stability of NOSC$_8$-900 in ORR was evaluated by chronoamperometric measurements at constant voltage of 0.45 V with a RDE rotating at 1600 rpm. For comparison, the activity of Pt/C (1 wt. %) was also measured in the same way. Whereas Pt/C (1 wt. %) exhibits ~25% loss of catalytic activity over 12 h, NOSC$_8$-900 shows only a slight loss of activity over the same time period (Figure S18). This clearly shows that NOSC$_8$-900 is quite stable as electrocatalyst. Moreover, methanol crossover test over NOSC$_8$-900 (SI) shows that the original cathodic ORR current of the catalyst remains almost unchanged (Figure S19), suggesting NOSC$_8$-900's high electrocatalytic selectivity for ORR. However, a similar test with Pt/C (1 wt. %) reveals that the electrocatalytic activity of this material for ORR significantly suffers after an addition of methanol into the solution (Figure S19). This remarkable tolerance exhibited by NOSC$_8$-900 against methanol crossover reaction suggests NOSC's lower activation barrier for ORR compared with that for methanol oxidation.[21]

Besides their electrocatalytic activity towoard ORR, NOSCs are found to exhibit catalytic activity toward AOR, with activities dependent on the amount of TBHP (oxidant) used (Table S4 and Figure S20). To the best of our knowledge, this is the first time heteroatom-doped nanocarbons are shown to catalyze AOR on their own. The results further show that benzyl alcohols with the electron-withdrawing $-NO_2$ group on *p*-position (i.e., *p*-nitrobenzyl alcohol) gives the highest conversion (~100% over 6 h, see Table S4), but with moderate selectivity (because of the faster overoxidation of aldehyde to acid). On the other hand, the *p*-substituted alcohol with electron-donating group ($-OMe$) gives excellent selectivity to aldehyde products, but with relatively lower conversion. NOSC$_8$-900 catalyzes also oxidation of secondary alcohols; and in fact, it does so at a faster rate than it does the corresponding primary alcohols (see Table S4). Additionally, the NOSC materials can easily be recovered at the end of the reactions and recycled for at least three runs without any significant loss of activity or selectivity (Figure S21); so, they are also stable under AOR.

In summary, we have described the synthesis of N-, O-, and S-tridoped, PPY-derived nanoporous carbons that exhibit efficient

and selective electrocatalytic and catalytic activity for ORR and AOR, respectively.

■ ASSOCIATED CONTENT

Ⓢ Supporting Information

Experimental details and supporting results. This material is available free of charge via the Internet at http://pubs.acs.org.

■ AUTHOR INFORMATION

Corresponding Authors
tasefa@rci.rutgers.edu
zwliu@scut.edu.cn

Notes

The authors declare no competing financial interest.

■ ACKNOWLEDGMENTS

■ REFERENCES

(1) Ibele, M. E.; Wang, Y.; Kline, T. R.; Mallouk, T. E.; Sen, A. *J. Am. Chem. Soc.* **2007**, *129*, 7762.

(2) Silva, R.; Voiry, D.; Chhowalla, M.; Asefa, T. *J. Am. Chem. Soc.* **2013**, *135*, 7823.

(3) (a) Gong, K.; Du, F.; Xia, Z.; Durstock, M.; Dai, L. *Science* **2009**, *323*, 760. (b) Yang, W.; Fellinger, T. P.; Antonietti, M. *J. Am. Chem. Soc.* **2011**, *133*, 206. (c) Zou, X.; Huang, X.; Goswami, A.; Silva, R.; Sathe, B. R.; Mikmeková, E.; Asefa, T. *Angew. Chem., Int. Ed.* **2014**, *126*, 4461. (d) Zheng, Y.; Jiao, Y.; Chen, J.; Liu, J.; Liang, J.; Du, A.; Zhang, W.; Zhu, Z.; Smith, S. C.; Jaroniec, M.; Lu, G. Q.; Qiao, S. Z. *J. Am. Chem. Soc.* **2011**, *133*, 20116.

(4) Yang, Z.; Yao, Z.; Li, G.; Fang, G.; Nie, H.; Liu, Z.; Zhou, X.; Chen, X.; Huang, S. *ACS Nano* **2012**, *6*, 205.

(5) Liang, H.-W.; Wei, W.; Wu, Z.-S.; Feng, X.; Müllen, K. *J. Am. Chem. Soc.* **2013**, *135*, 16002.

(6) Maeda, S.; Armes, S. P. *J. Mater. Chem.* **1994**, *4*, 935.

(7) Motiei, M.; Hacohen, Y. R.; Calderon-Moreno, J.; Gedanken, A. *J. Am. Chem. Soc.* **2001**, *123*, 8624.

(8) Yang, S.; Zhi, L.; Tang, K.; Feng, X.; Maier, J.; Müllen, K. *Adv. Funct. Mater.* **2012**, *22*, 3634.

(9) Qu, L.; Liu, Y.; Baek, J. B.; Dai, L. *ACS Nano* **2010**, *4*, 1321.

(10) Liang, J.; Jiao, Y.; Jaroniec, M.; Qiao, S. Z. *Angew. Chem., Int. Ed.* **2012**, *51*, 11496.

(11) Mattevi, C.; Eda, G.; Agnoli, S.; Miller, S.; Mkhoyan, K. A.; Celik, O.; Mastrogiovanni, D.; Granozzi, G.; Garfunkel, E.; Chhowalla, M. *Adv. Funct. Mater.* **2009**, *19*, 1.

(12) Chung, H. T.; Won, J. H.; Zelenay, P. *Nat. Commun.* **2013**, *4*, 1922.

(13) Li, Y.; Zhou, W.; Wang, H.; Xie, L.; Liang, Y.; Wei, F.; Idrobo, J.-C.; Pennycook, S. J.; Dai, H. *Nature* **2012**, *7*, 394.

(14) Seredych, M.; Bandosz, T. J. *Carbon* **2014**, *66*, 227.

(15) Wang, S.; Yu, D.; Dai, L. *J. Am. Chem. Soc.* **2011**, *133*, 5182.

(16) Liang, Y.; Li, Y.; Wang, H.; Zhou, J.; Wang, J.; Regier, T.; Dai, H. *Nat. Mater.* **2011**, *10*, 780.

(17) (a) Liang, J.; Du, X.; Gibson, C.; Du, X. W.; Qiao, S. Z. *Adv. Mater.* **2013**, *25*, 6226. (b) Groot, M.T. de; Merkx, M.; Wonders, A. H.; Koper, M. T. M. *J. Am. Chem. Soc.* **2005**, *127*, 7579.

(18) Olson, T. S.; Pylypenko, S.; Fulghum, J. E.; Atanassov, P. *J. Electrochem. Soc.* **2010**, *157*, B54.

(19) (a) Simonet, J. *Electrochem. Commun.* **2013**, *34*, 223. (b) Wang, D.-W.; Su, D. *Energy Environ. Sci.* **2014**, *7*, 576.

(20) Cheon, J. Y.; Kim, J. H.; Kim, J. H.; Goddeti, K. C.; Park, J. Y.; Joo, S. H. *J. Am. Chem. Soc.* **2014**, *136*, 8875.

(21) Wang, S.; Yu, D.; Dai, L.; Chang, D.-W.; Baek, J.-B. *ACS Nano* **2011**, *5*, 6202.